

## Article

# The Effects on Thermal Efficiency of Yttria-Stabilized Zirconia and Lanthanum Zirconate-Based Thermal Barrier Coatings on Aluminum Heating Block for 3D Printer

Hasan Demir 

Ortakoy Vocational School, Aksaray University, Aksaray 68300, Turkey; hasandemir@aksaray.edu.tr;  
Tel.: +09-038-2288-3817

**Abstract:** Fused filament fabrication is an important additive manufacturing method, for which 3D printers are the most commonly used printing tools. In this method, there are many factors that affect the printing quality, chief among which is temperature. The fusion temperature of the material is created by an aluminum heating block in the extruder. Stability and a constant temperature for the aluminum heating block are inevitable requirements for print quality. This study aims to use the thermal barrier coating method to increase the thermal efficiency and stability of the aluminum heating block by reducing heat loss. Furthermore, it aims to perform steady-state thermal analysis using finite element analysis software. The analyses are carried out in stagnant air environment and at the printing temperature of acrylonitrile butadiene styrene material. In order to examine the effects of different coating materials, blocks coated with two different coating materials, as well as uncoated blocks, were used in the analyses. The coating made with yttria-stabilized zirconia and pyrochlore-type lanthanum zirconate materials, together with the NiCrAl bond layer, prevent temperature fluctuation by preventing heat loss. The effects of the coating method on average heat flux density, temperature distribution of blocks, and temperature distribution of the filament tube hole were investigated. Additionally, changes in flow velocity were determined by examining the effects of the thermal barrier coating method on temperature distribution. The average heat flux density in the coated blocks decreased by 10.258%. Throughout the investigation, the temperature distributions in the coated blocks became homogeneous. It was also observed that both coating materials produce the same effect. This article performs a steady-state thermal analysis of a conventional model and thermal-barrier-coated models to increase print quality by reducing heat loss from the aluminum heating block.



**Citation:** Demir, H. The Effects on Thermal Efficiency of Yttria-Stabilized Zirconia and Lanthanum Zirconate-Based Thermal Barrier Coatings on Aluminum Heating Block for 3D Printer. *Coatings* **2021**, *11*, 792. <https://doi.org/10.3390/coatings11070792>

Academic Editor: Dana Ashkenazi

Received: 4 June 2021

Accepted: 29 June 2021

Published: 30 June 2021

**Publisher's Note:** MDPI stays neutral with regard to jurisdictional claims in published maps and institutional affiliations.



**Copyright:** © 2021 by the author. Licensee MDPI, Basel, Switzerland. This article is an open access article distributed under the terms and conditions of the Creative Commons Attribution (CC BY) license (<https://creativecommons.org/licenses/by/4.0/>).

**Keywords:** aluminum heating block; NiCrAl; La<sub>2</sub>Cr<sub>2</sub>O<sub>7</sub>; yttria-stabilized zirconia; 3D printer; ANSYS

## 1. Introduction

Fused filament fabrication (FFF) has become an important additive manufacturing (AM) method. This technique has many advantages, including rapid prototyping, flexible production, and ease of use [1–4], but it has not yet been fully adopted by the FFF manufacturing industry. Due to its advantages, medical doctors, students, and artists use this production technique for rapid prototyping. FFF production technology is most often referred to as 3D printing [3,5–11].

Three-dimensional printers are machines used in FFF production. In the printing process, a solid filament, such as polylactic acid (PLA) and acrylonitrile butadiene styrene (ABS), is melted and extruded from a nozzle [1,12–14]. During the printing process in 3D printers, the filament is left layer by layer as it diffuses with the effect of the temperature [15,16]. Proper diffusion depends on the printing temperature [11,17]. The stability of the printing temperature, according to filament type, ensures full fusion and successful diffusion [18,19]. The printing temperature is formed within the aluminium heating block (AHB), which is heated by the heater element. The task of AHB is to ensure the stability of

the thermal regime. The filament passing through the AHB, as shown in Figure 1, fuses and comes out of the nozzle. Changes in the working environment of the 3D printer, such as the filament speed, which depends on the printing speed, can cause the temperature of the AHB to fluctuate [4]. For example, the perimeter of the part is usually printed at low speeds, while the infill is printed at higher speeds. This change in filament speed causes the temperature to fluctuate. The fluctuation in the temperature and the instability of the desired value prevent the fusion from occurring completely and cause the printing process to deteriorate, creating faults in the manufactured part [20]. To prevent temperature fluctuation, a coating method with a material that has a low heat conduction coefficient, to protect the parts of gas turbine engines from high temperatures, can be used.



**Figure 1.** The commercially used AHB.

Thermal barrier coating (TBC) is a high material system used to provide thermal insulation for parts of a system exposed to high temperatures, such as internal combustion engines and gas turbines [21,22]. TBC was first developed in NASA laboratories in the 1950s. The aim of the thermal barrier is to protect the parts from the temperature outside of the system, as well as to increase the hot corrosion resistance of the system's parts [23,24]. TBCs are ceramic-based materials that resist high temperatures better than metals [25,26]. There are coating materials under development, such as gadolinium zirconate ( $Gd_2Zr_2O_7$ ), pyrochlore-type lanthanum zirconate ( $La_2Zr_2O_7$ ), as well as the commercial coating yttria-stabilized zirconia (YSZ), which is widely used. Coatings have low thermal conductivity and mainly serve to reduce heat transfers [27,28]. The acceptable thickness level of a TBC is between 0.2 and 0.8 mm. A bond coat is applied in between the TBC and the substrate surface to adhere. By reducing the difference in thermal expansion between the substrate surface and the ceramic-based TBC, the bond coat increases the service life of the TBC. Additionally, it creates the rough surface required for the adhesion of the TBC [24]. The bond coat also has the task of preventing oxidation from reaching the substrate surface.

Today, the most widely used coating at high temperatures is YSZ. It can be used at temperatures of up to 1200 °C and has high thermal shock resistance. The main material of YSZ is zirconium. Zirconium ( $Zr^{4+}$ ) is used as a TBC due to its low thermal conductivity. Since zirconium has three crystal forms, it cannot be used alone as a TBC. Oxide forms of calcium (Ca), magnesium (Mg), and yttrium (Y) are used to stabilize zirconium. Figure 2a shows the crystal structure of zirconium stabilized with yttrium oxide. Figure 2b shows SEM micrographs of zirconium with improved mechanical and thermal properties stabilized with yttrium [29–31].

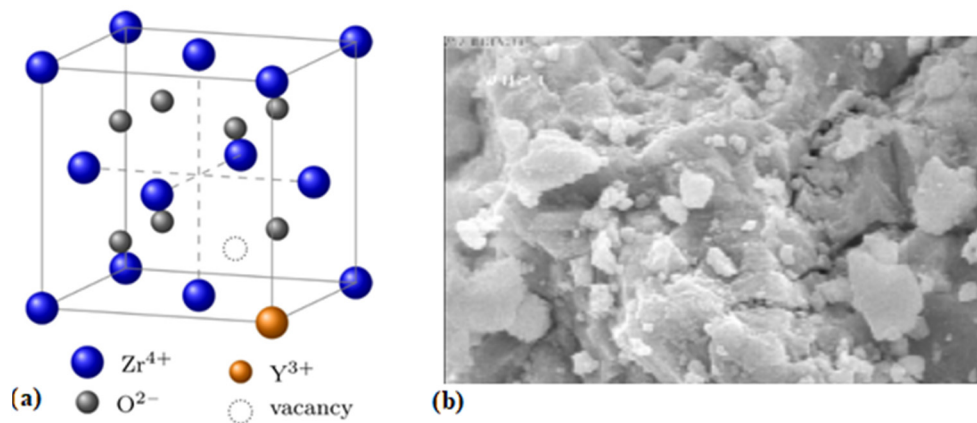


**Figure 2.** (a) Illustration of the yttria-stabilized zirconia structure [30], (b) SEM micrographs of YSZ at high temperature [29].

$\text{La}_2\text{Cr}_2\text{O}_7$  has been proposed as an alternative ceramic-based compound to YSZ, as it can operate at higher temperatures. It has no phase change up to 2000 °C. There are atoms of three different chemical elements in the  $\text{La}_2\text{Cr}_2\text{O}_7$  structure, which is shown in Figure 3a. It can be seen that  $\text{La}_2\text{Cr}_2\text{O}_7$  particles, a SEM image of which appears in Figure 3b, are well crystallized.  $\text{La}_2\text{Cr}_2\text{O}_7$  has a lower thermal conductivity and thermal expansion coefficient than YSZ. However, since the thermal expansion coefficient of the substrate material and the bond layer is higher than  $\text{La}_2\text{Cr}_2\text{O}_7$ , it causes internal stresses and cracks in TBC, thus reducing the coating life [32–34].

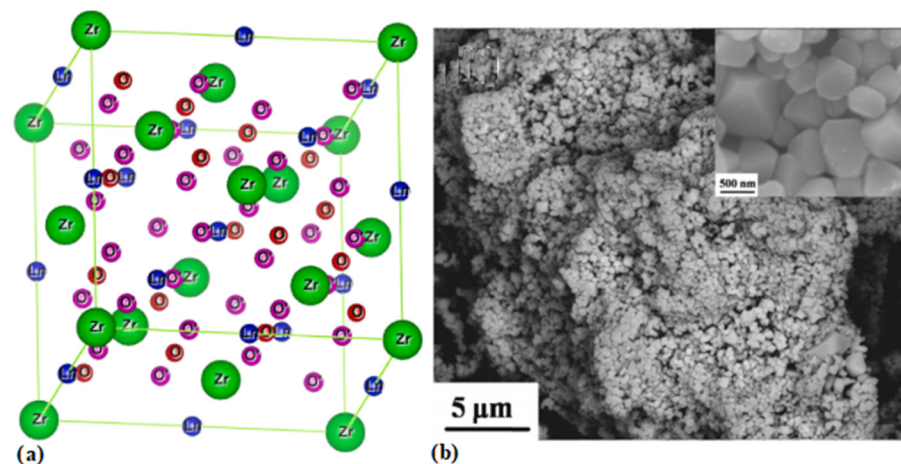


**Figure 3.** (a) Illustration of the  $\text{La}_2\text{Cr}_2\text{O}_7$  [32] (Permission from [32] Copyright 2021 Elsevier), (b) SEM micrographs of  $\text{La}_2\text{Cr}_2\text{O}_7$  at high temperature [33] (Permission from [33] Copyright 2016 Elsevier).

In this study, steady-state thermal analysis of TBC-coated AHB and uncoated AHB, using the finite element method (FEM), were compared. Yttria-stabilized zirconia and  $\text{La}_2\text{Cr}_2\text{O}_7$  materials were used in simulations due to their different thermal and mechanical properties. The preservation of a thermal regime and ensuring a stable operating temperature by preventing heat loss from the AHB with TBCs were investigated. We examined the temperature distribution of the filament tube hole where the filament fused, and the effect of TBCs on temperature distribution was also determined. A comparison between coated and uncoated models was made by examining the average heat transfer per unit area. The contribution of TBCs to the thermal efficiency and printing process was successfully demonstrated in the present study.

## 2. Materials and Simulation

### 2.1. Materials

Conventionally, AHBs are fabricated from aluminum alloys. AHBs, which are produced in various dimensions and shapes, are used in AM processes. The AHB model, which uses a commercial 3D printer device (Leapfrog HS Creatr, Alphen aan den Rijn, Netherlands), was used in the simulations. The dimensions of the AHB which form the substrate surface were  $20 \times 18 \times 10$  mm, and the coated and uncoated AHB models are shown in Figure 4. After a literature review, the bond layer material was determined as NiCrAl [28,35]. The thickness of the bond layer under the ceramic coating was 0.15 mm. Analyses were performed by determining the material of TBC, and its thickness was 0.5 mm. Figure 5 shows the layers that comprise the TBC. Table 1 shows the properties of the TBC materials and the bond layer material used in this study [21].

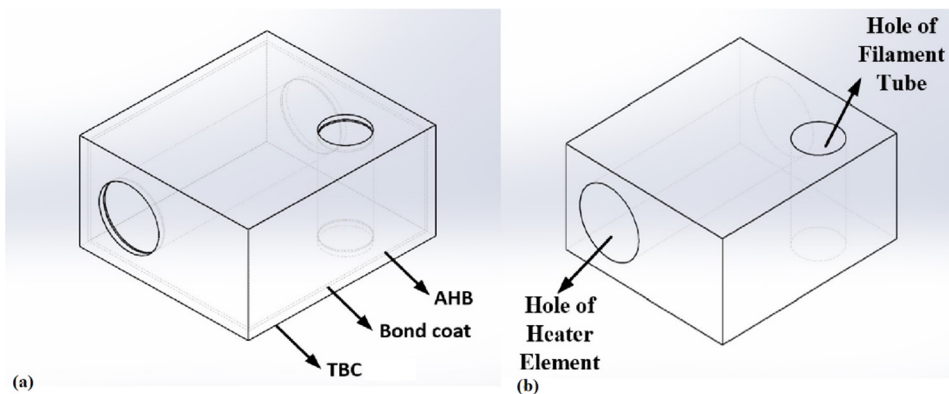


Figure 4. (a) The coated and (b) uncoated AHB models.

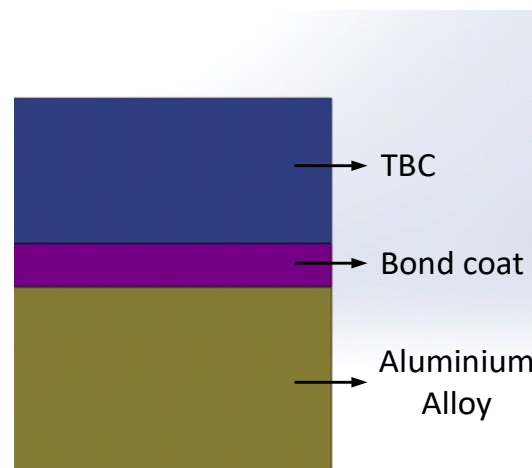


Figure 5. Layers in the thermal barrier coating for the AHB.

Table 1. Thermal properties of materials [21].

Material	Thermal Conductivity (W/m K)	Thermal Expansion $\times 10e-6$ (1/K)	Specific Heat (J/kg K)
NiCrAl	16.1	12	764
YSZ	2.2	10.9	620
La <sub>2</sub> Cr <sub>2</sub> O <sub>7</sub>	1.5	9.5	N/A

### 2.2. Numerical Modeling of the Thermal Problem

The second law of thermodynamics states that heat flows spontaneously from a hot source to a cold source. The movement of heat causes the temperature of objects to change

and reach an equilibrium. The temperature changes in bodies over time are described by Newton's law of cooling and is expressed in Equation (1):

$$\frac{dT(t)}{dt} = -k(T(t) - T_{\infty}), \quad (1)$$

where  $T(t)$  is the temperature at time  $t$ ,  $k$  is the temperature changing coefficient, and  $T_{\infty}$  is the environmental temperature.

Heat is transferred in three different ways: conduction, convection, and radiation. In this study, heat transfer by conduction and convection was investigated. Heat conduction occurs between the layers of the AHB with a thermal barrier coating. Heat transfer by conduction is based on Newton's law of cooling and is expressed in Equation (2):

$$Q_{cond} = kA(T_s - T_{\infty}), \quad (2)$$

where  $k$  is the thermal conductivity of the material,  $A$  is the surface area through which heat transfer takes place, and  $T_s$  is the surface temperature.

Since both coated and uncoated AHBs are in a stagnant (non-flowing) air environment, heat transfer occurs by convection from their surfaces when they come into contact with air. Heat transfer by convection is expressed in Equation (3):

$$Q_{conv} = hA(T_s - T_{\infty}), \quad (3)$$

where  $h$  is the convection heat transfer coefficient.

When conduction and convection heat transfers (Equations (2) and (3)) are examined, it is clear that the heat transfer depends on the coefficients of the material and the temperature difference. Based on this, the current study aims to reduce heat transfer by using materials with different thermal properties. Using different materials was expected to prevent heat transfer by changing the heat transfer coefficients, while simultaneously changing the temperature of the surfaces.

### 2.3. Simulation of Finite Element Analysis

Steady-state thermal analyses were performed to calculate the effect of the thermal barrier coatings on the AHB. Average heat transfers at steady-state temperature were investigated for both the coated and uncoated AHBs. The finite element analysis software ANSYS was used in the analyses. The coated AHB consists of three layers—substrate, bond coat, and TBC—and inter-surface contact was defined for each layer. The major mechanism of heat transfers between TBC surface and the air occurred as convection. In addition, for the coated AHB, heat transfers occurred according to the thermal properties given in Table 1, due to contact between each layer. There were two boundary conditions between air and model in this study:

- The ambient temperature was 22 °C and the air was stagnant. The heat transfer coefficient was 5 W/m<sup>2</sup> K between AHB and air;
- Since the printing temperature for ABS material was 260 °C, the AHB temperature was 260 °C due to the extruder temperature.

### Mesh and Convergence Study

A convergence study was carried out using heat flux density. The FEM was simulated for six different meshes, each one increasing the number of elements, from extremely coarse to normal. As shown in Figure 6, the mesh convergence for coated and uncoated AHB models occurs over 10,000 and 20,000, respectively. As a result of convergence, meshing of AHB models was achieved with skewness. Skewness mesh spectrum expresses mesh quality between 0 and 1, according to average skewness quality. The number of elements and average skewness quality of the coated and uncoated AHBs are given in Table 2. A single-coated AHB model was used for the YSZ and La<sub>2</sub>Cr<sub>2</sub>O<sub>7</sub> coating. According to the

skewness mesh spectrum, the average skewness quality of both models is between 0.25 and 0.5, confirming that the quality of the mesh used in this study is high.

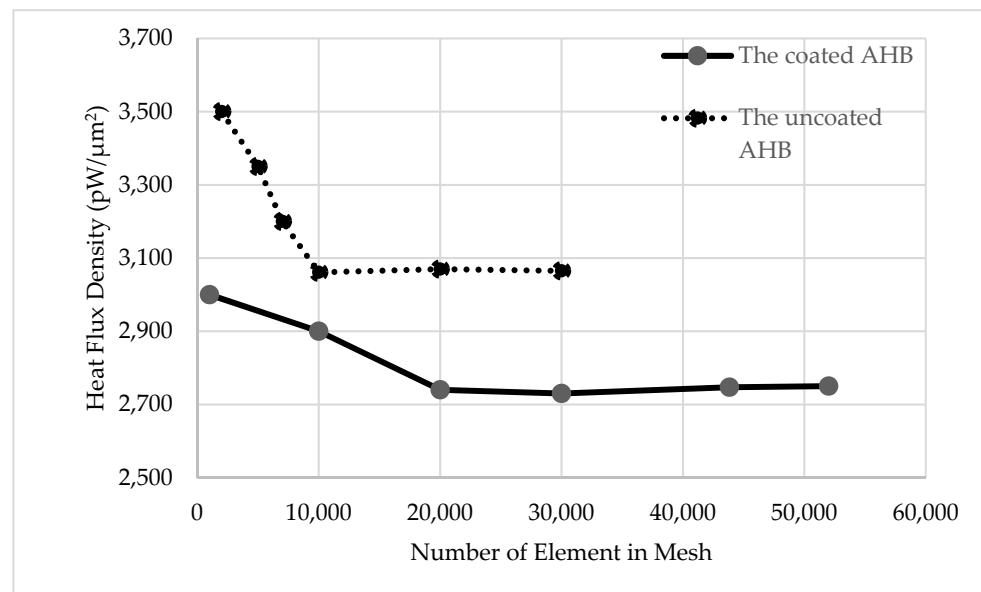


Figure 6. Mesh convergence study based on the heat flux density.

Table 2. The number of elements and average skewness quality.

Material	Number of Elements	Average Skewness Quality
Uncoated AHB	10,053	0.28612
Coated AHB	43,825	0.37147

### 3. Results and Discussion

Steady-state thermal analysis was performed with the specified boundary conditions and thermal properties in reference [21]. For coated and uncoated AHBs, temperature distribution, temperature distribution of filament tube hole, heat flux density, and average heat flux density were obtained. The temperature distribution is given in Figure 7. It was observed that the maximum temperature was in the heating element hole, which formed the heat source in both models. When the surface temperatures of the models were observed, it was found that the temperature reaching 260 °C in the uncoated model was not homogeneously distributed. When the YSZ and La<sub>2</sub>Cr<sub>2</sub>O<sub>7</sub> coatings were compared, it was found that the surface temperature of the La<sub>2</sub>Cr<sub>2</sub>O<sub>7</sub>-coated AHB model was approximately 0.5 °C lower. It was determined that there was no significant difference between the surface temperatures of the coatings. This is because the conduction provided in Equation (2) depends on the conduction coefficient of heat transfer and the coefficients of both coating materials being close to each other.

In the coated models, while the temperature did not reach 260 °C at any point on the surface, a more homogeneous temperature distribution was observed, as shown in the cross-sectional view in Figure 8b,c. In addition, when the temperature distribution of the filament tube was examined, the temperature was higher in the coated models. In this case, it was observed that the temperature of the filament tube increased because the surface temperature was lowered, and the temperature distribution was homogeneous in the coated models. This is the most striking result of the simulation. Heat loss from the surface of the AHB to the outside environment was prevented and directed to the filament tube hole in the AHB by the coating. By directing the heat to the filament tube hole in the coated models, the fusion process can be faster and the heating time can be shortened.

Moreover, temperature fluctuations due to printing parameters, such as filament speed and environment variables, can be prevented by avoiding heat loss.

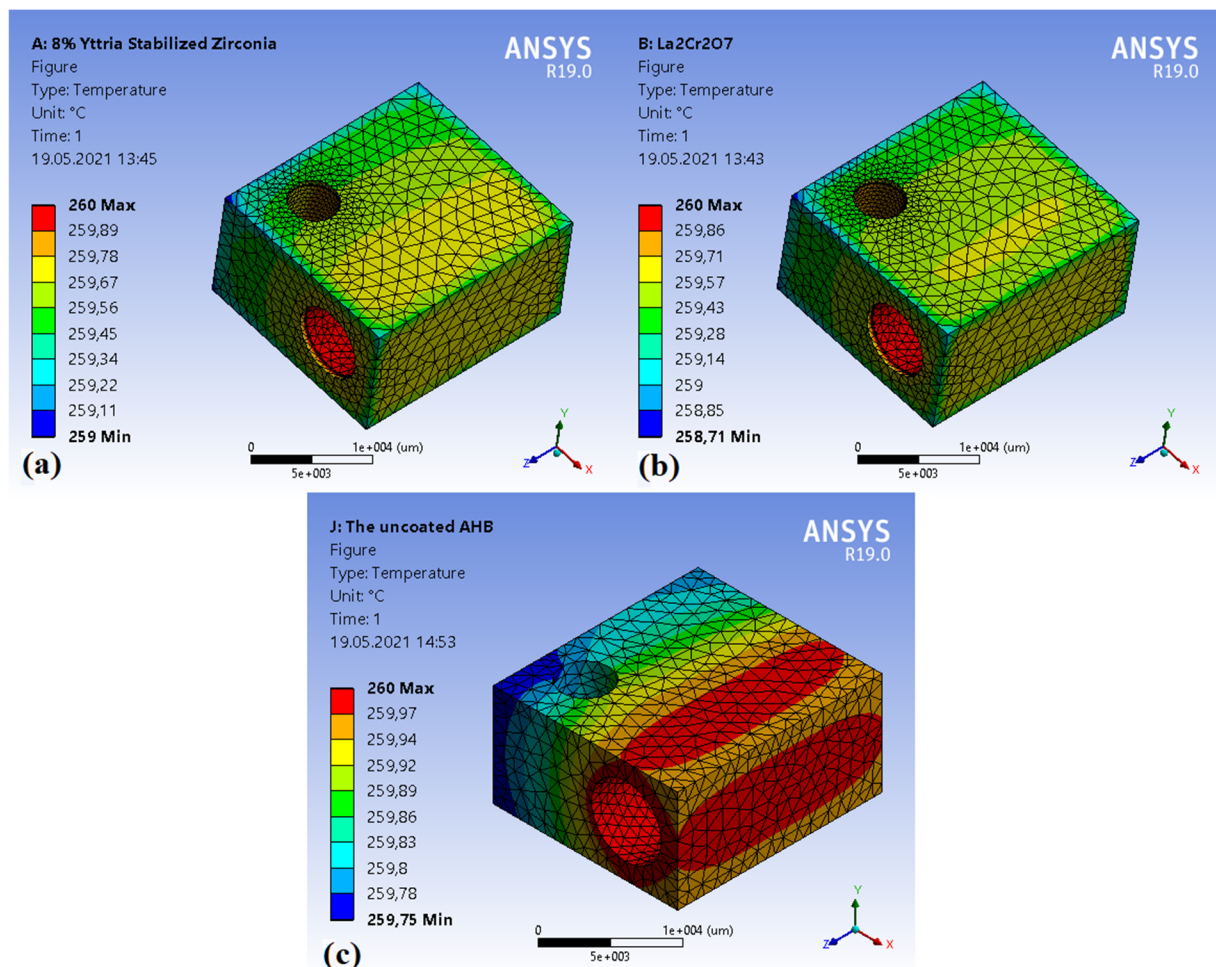


**Figure 7.** Temperature distribution of (a) YSZ-coated, (b) La<sub>2</sub>Cr<sub>2</sub>O<sub>7</sub>-coated, and (c) uncoated AHB.

When the cross-sectional views of TBC materials given in Figure 8b,c were compared, it was found that La<sub>2</sub>Cr<sub>2</sub>O<sub>7</sub> is more homogenous than YSZ. However, there is no striking difference between the two materials. Although the TBC materials do not differ from each other, their advantages in temperature distribution compared to the uncoated model are obvious. The homogeneous temperature distribution in the filament tube hole of the coated models will ensure that the filament fusion is equal in every region. In reference [4], the melt filament flow profile in the extruder was investigated according to viscosity, extrusion speed, and shear rate. As the extrusion velocity increases, the residence time of the filament in AHB decreases. Therefore, heat transfer from AHB to filament will be reduced and the flow velocity will be adversely affected. Generally, polymer materials are used as filaments and have high viscosity values. The inhomogeneous temperature distribution of the filament tube hole in the uncoated AHB creates turbulence in the flow, as seen in Figure 9a, due to the high viscosity of the filament. Since the temperature distribution around the filament tube hole of the coated models was homogeneous, the viscosity of the polymer material is the same in every region. Therefore, the flow velocity profile is regular, and the flow is a laminar flow, as shown in Figure 9b [4]. TBC contributes to the formation of laminar flow, which is the ideal flow profile.

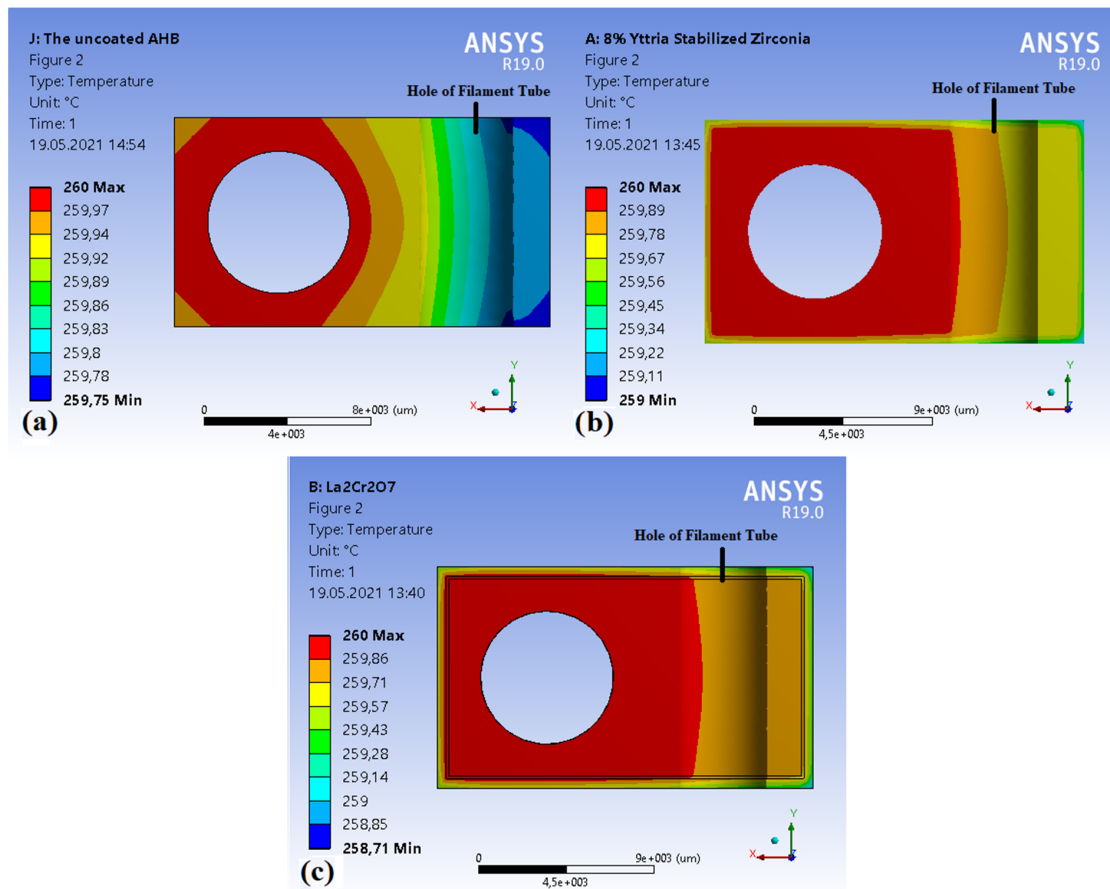


Figure 8. Cross-sectional view of the temperature distribution of (a) uncoated, (b) YSZ-coated, and (c) La<sub>2</sub>Cr<sub>2</sub>O<sub>7</sub>-coated. AHB.

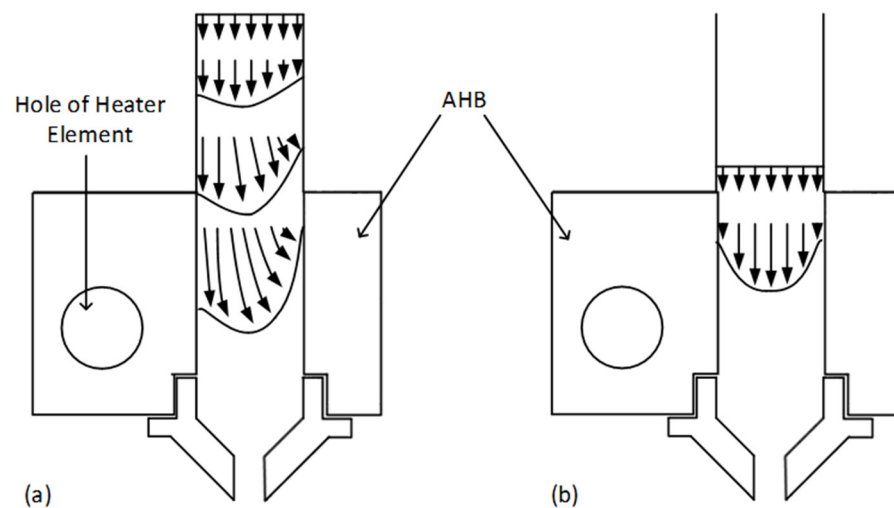


Figure 9. Schematic flow-velocity profile of (a) uncoated AHB and (b) coated AHB.

The minimum surface temperatures between the layers of coated AHB are given in Figure 10. Through the literature, it was found that the surface temperature ( $T_s$ ) of AHB was reduced by the thermal barrier [26]. By reducing the difference between the surface temperature of the TBC ( $T_{TBC}$ ) and the ambient temperature ( $T_\infty$ ), heat transfer by convection was reduced. As shown in Figure 10, the surface temperatures of both coating materials were close to each other. By preventing heat loss into the environment,

it was ensured that the temperature of the filament tube hole was increased, as shown in Figure 8b,c.

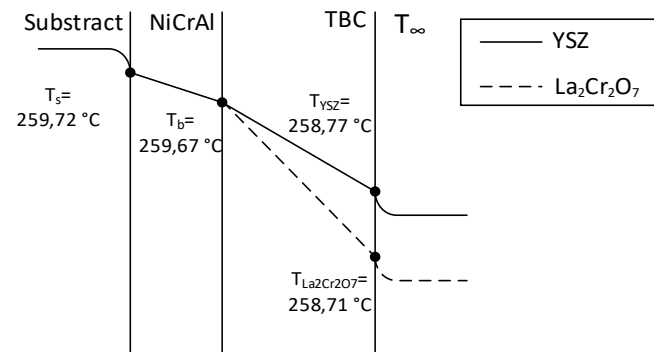


Figure 10. Surface temperature of coated AHB.

The heat flux realized by convection between the air and the surfaces of the models, both coated and uncoated AHB, is shown in Figure 11. When the heat flow of the uncoated model was examined, it was seen that there is heat loss around the filament tube hole. This scenario reduced the temperature required for fusion, and therefore affects the print quality. It was observed that the heat transfer on the coated models' surfaces was lower due to TBC. While the average heat flux density in the uncoated model was 3061 W/m<sup>2</sup>, the average heat flux density of YSZ and La<sub>2</sub>Cr<sub>2</sub>O<sub>7</sub> was 2747 W/m<sup>2</sup> and 2746.6 W/m<sup>2</sup>, respectively. For the average heat flux density, it was observed that the heat transferred from the models with TBC to the working environment was 10.258% less than the uncoated model.

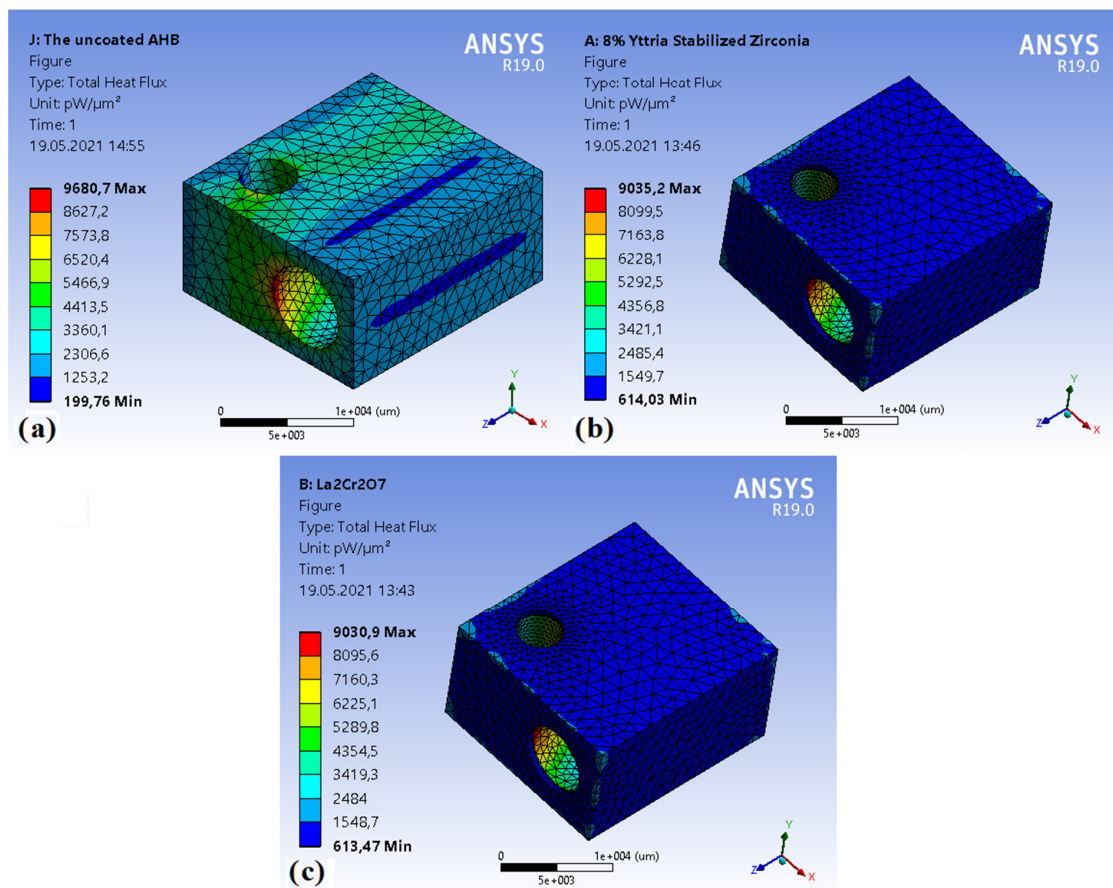


Figure 11. Heat flux density of (a) uncoated, (b) YSZ-coated, and (c) La<sub>2</sub>Cr<sub>2</sub>O<sub>7</sub>-coated AHB.

There is no difference in the average heat flux density of both coating materials. The most important reason for this is that the thermal conductivity of the materials is very close for each, and therefore the difference between the surface temperature and the ambient temperature is low. If the working temperature of AHB is higher than 260 °C, the low thermal conductivity of LA material will be more apparent.

To conclude the numerical simulation, the surface temperature, cross-sectional views, and average heat flux density of AHB models were recorded. It was found that AHB models with TBC made of temperature-resistance materials lose less heat than the uncoated model. However, it has been determined that both coating materials show the same effect due to the low operating temperature of the AHB. In addition, when the temperature distributions for the models were examined, it was observed that the temperature of the filament tube hole of the models applied with the TBC method was higher.

#### 4. Conclusions

In this article, steady-state thermal analysis was performed to increase the thermal efficiency of the AHB, which provided a stable fusion temperature in 3D printers, using the TBC coating method. The TBC method, which can withstand high temperatures due to its low thermal conductivity, was used in this study to reduce heat loss. As a result of the analysis, we can draw the following conclusions:

- The operating temperature of the AHB is lower than the maximum operating temperature of TBC materials. Therefore, thermal expansion and crack formation caused by temperature will be reduced [34]. Due to the low thermal expansion coefficient of YSZ, it will have a longer life than  $\text{La}_2\text{Cr}_2\text{O}_7$ . The validity of using the coating method for 3D printers operating at high temperatures (approximately 500 °C) requires further experimental studies;
- YSZ and  $\text{La}_2\text{Cr}_2\text{O}_7$  coatings showed the same effects in preventing heat loss. Both coating materials are suitable for use at 260 °C. However, at higher temperatures, the difference between the thermal conductivity of the materials will be apparent. Cracks will occur on the material surfaces and their service life will be reduced [34]. In future studies, these effects could be examined through analysis and experiments that can be conducted at high temperatures;
- The effect of the coating method on the melt flow velocity was investigated. The homogeneous temperature distribution of the coated models provided the flow velocity of the filament with a regular profile. It was found that TBC contributes to a laminar flow;
- TBC prevented heat loss. It contributed to the homogeneous distribution of heat on AHB;
- TBC affected the distribution of temperature on AHB by preventing heat loss. The temperature of the filament tube hole increased;
- The transfer of heat to the surrounding environment was prevented, and the heating time of AHB was shortened;
- Energy losses were prevented by increasing thermal efficiency. With the closed loop control method, when the temperature of the AHB decreases the heating element operates, and heating is provided. Reducing the heat flux prevents temperature fluctuations and the heater element works less. This reduces the energy consumption required for heating.

The numerical analysis showed a dramatic change in the average heat flux density due to TBC. It was found that the average heat flux density was reduced by 10.258% and that thermal efficiency was increased by coating. By increasing the thermal efficiency, the protection of the thermal regime was easier than it was for the uncoated model. This scenario makes 3D printer temperature control methods easier. Furthermore, it increases the printing quality and reduces printing faults by ensuring the full realization of filament fusion with increased thermal efficiency and high thermal stability.

**Funding:** The author did not receive any specific funding for this work.

**Institutional Review Board Statement:** Not applicable.

**Informed Consent Statement:** Not applicable.

**Data Availability Statement:** Not applicable.

**Conflicts of Interest:** The author declares no conflict of interest.

## References

1. McIlroy, C.; Olmsted, P.D. Disentanglement effects on welding behaviour of polymer melts during the fused-filament-fabrication method for additive manufacturing. *Polymer* **2017**, *123*, 376–391. [[CrossRef](#)]
2. Turner, B.N.; Gold, S.A. A review of melt extrusion additive manufacturing processes: II. Materials, dimensional accuracy, and surface roughness. *Rapid Prototyp. J.* **2015**, *21*, 250–261. [[CrossRef](#)]
3. Wong, K.V.; Hernandez, A. A Review of Additive Manufacturing. *ISRN Mech. Eng.* **2012**, *2012*, 1–10. [[CrossRef](#)]
4. Peng, F.; Vogt, B.D.; Cakmak, M. Complex flow and temperature history during melt extrusion in material extrusion additive manufacturing. *Addit. Manuf.* **2018**, *22*, 197–206. [[CrossRef](#)]
5. Horn, T.J.; Harrysson, O.L.A. Overview of current additive manufacturing technologies and selected applications. *Sci. Prog.* **2012**, *95*, 255–282. [[CrossRef](#)] [[PubMed](#)]
6. Guo, N.; Leu, M.C. Additive manufacturing: Technology, applications and research needs. *Front. Mech. Eng.* **2013**, *8*, 215–243. [[CrossRef](#)]
7. Vaezi, M.; Seitz, H.; Yang, S. A review on 3D micro-additive manufacturing technologies. *Int. J. Adv. Manuf. Technol.* **2013**, *67*, 1721–1754. [[CrossRef](#)]
8. Turner, B.N.; Strong, R.; Gold, S.A. A review of melt extrusion additive manufacturing processes: I. Process design and modeling. *Rapid Prototyp. J.* **2014**, *20*, 192–204. [[CrossRef](#)]
9. Parandoush, P.; Lin, D. A review on additive manufacturing of polymer-fiber composites. *Compos. Struct.* **2017**, *182*, 36–53. [[CrossRef](#)]
10. Vukicevic, M.; Mosadegh, B.; Min, J.K.; Little, S.H. Cardiac 3D Printing and Its Future Directions. *JACC Cardiovasc. Imaging* **2017**, *10*, 171–184. [[CrossRef](#)]
11. Dizon, J.R.C.; Espera, A.H.; Chen, Q.; Advincula, R.C. Mechanical characterization of 3D-printed polymers. *Addit. Manuf.* **2018**, *20*, 44–67. [[CrossRef](#)]
12. Enrique, L.; Vega-rios, A. Filament extrusion and its 3D printing of poly (lactic acid)/poly (styrene-Co-methyl methacrylate) blends. *Appl. Sci.* **2019**, *9*, 5153. [[CrossRef](#)]
13. Gregor-Svetec, D.; Leskovšek, M.; Vrabič Brodnjak, U.; Stankovič Elesini, U.; Muck, D.; Urbas, R. Characteristics of HDPE/cardboard dust 3D printable composite filaments. *J. Mater. Process. Technol.* **2020**, *276*, 116379. [[CrossRef](#)]
14. Singh, R.; Singh, G.; Singh, J.; Kumar, R. Investigations for tensile, compressive and morphological properties of 3D printed functional prototypes of PLA-PEKK-HAp-CS. *J. Thermoplast. Compos. Mater.* **2019**. [[CrossRef](#)]
15. Comminal, R.; Serdeczny, M.P.; Pedersen, D.B.; Spangenberg, J. Numerical modeling of the strand deposition flow in extrusion-based additive manufacturing. *Addit. Manuf.* **2018**, *20*, 68–76. [[CrossRef](#)]
16. Osswald, T.A.; Puentes, J.; Kattinger, J. Fused filament fabrication melting model. *Addit. Manuf.* **2018**, *22*, 51–59. [[CrossRef](#)]
17. Chacón, J.M.; Caminero, M.A.; García-Plaza, E.; Núñez, P.J. Additive manufacturing of PLA structures using fused deposition modelling: Effect of process parameters on mechanical properties and their optimal selection. *Mater. Des.* **2017**, *124*, 143–157. [[CrossRef](#)]
18. Fleck, T.J.; Murray, A.K.; Gunduz, I.E.; Son, S.F.; Chiu, G.T.C.; Rhoads, J.F. Additive manufacturing of multifunctional reactive materials. *Addit. Manuf.* **2017**, *17*, 176–182. [[CrossRef](#)]
19. Bellehumeur, C.; Li, L.; Sun, Q.; Gu, P. Modeling of bond formation between polymer filaments in the fused deposition modeling process. *J. Manuf. Process.* **2004**, *6*, 170–178. [[CrossRef](#)]
20. Yang, C.; Tian, X.; Li, D.; Cao, Y.; Zhao, F.; Shi, C. Influence of thermal processing conditions in 3D printing on the crystallinity and mechanical properties of PEEK material. *J. Mater. Process. Technol.* **2017**, *248*, 1–7. [[CrossRef](#)]
21. Manohar, B.; Jothi, M.; Udaykumar, R. The effects of thermal barrier coating on thermal stress and temperature distribution in a diesel engine piston for magnesia/yittria partially stabilized zirconia. *Int. J. Res. Mech. Eng. Technol.* **2015**, *6*, 9–15.
22. Aabid, A.; Khan, S.A. Optimization of heat transfer on thermal barrier coated gas turbine blade. *IOP Conf. Ser. Mater. Sci. Eng.* **2018**, *370*, 012022. [[CrossRef](#)]
23. Kumar, D.; Pandey, K.N.; Das, D.K. Thermal barrier coatings on aluminium-based alloy 2024 for high temperature protection subjected to thermal cyclic loading. *Procedia Mater. Sci.* **2014**, *5*, 1075–1080. [[CrossRef](#)]
24. Ciftiyürek, E. %8 YSZ (İtiryum İle Stabilize Edilmiş ZrO<sub>2</sub>) Termal Bariyer Kaplamaların (TBK) Üretilmesi ve Proses Parametreleri Optimizasyonu. Ph.D. Thesis, Istanbul Technical University, Istanbul, Turkey, 2009.
25. Yesildal, R.; Günay, Y.Z. The coating with plasma spray method and research of spray characteristics. *Deü Mühendislik Fakültesi Fen Ve Mühendislik Derg.* **2007**, *9*, 59–76.

26. Singh, G.; Bala, N.; Mishra, A. Comprehensive review on mcraly coatings: Structure, properties and future. *Int. J. Adv. Sci. Technol.* **2020**, *29*, 4867–4870.
27. Guven Gok, M.; Goller, G. State of the art of gadolinium zirconate based thermal barrier coatings: Design, processing and characterization. *Methods Film Synth. Coat. Proced.* **2020**. [[CrossRef](#)]
28. Diltemiz, S.F. Thermal and Mechanical Properties Optimisation of Thermal Barrier Coatings. Ph.D. Thesis, Eskisehir Osmangazi University, Eskisehir, Turkey, 2010.
29. Khaloobagheri, M.; Janipour, B.; Askari, N.; Shafiee Kamal Abad, E. Characterisation of powder metallurgy Cu-ZrO<sub>2</sub> composites. *Adv. Prod. Eng. Manag.* **2013**, *8*, 1–8. [[CrossRef](#)]
30. Vagner, P.; Gohlke, C.; Milos, V.; Müller, R.; Fuhrmann, J. A continuum model for yttria-stabilized zirconia incorporating triple phase boundary, lattice structure and immobile oxide ions. *J. Solid State Electrochem.* **2019**, *23*, 2907–2926. [[CrossRef](#)]
31. Hayashi, H.; Saitou, T.; Maruyama, N.; Inaba, H.; Kawamura, K.; Mori, M. Thermal expansion coefficient of yttria stabilized zirconia for various yttria contents. *Solid State Ion.* **2005**, *176*, 613–619. [[CrossRef](#)]
32. Kushwaha, A.K.; Mishra, S.P.; Vishwakarma, M.K.; Chauhan, S.; Jappor, H.R.; Khenata, R.; Bin Omran, S. Theoretical study of thermal conductivity, mechanical, vibrational and thermodynamical properties of Ln<sub>2</sub>Zr<sub>2</sub>O<sub>7</sub> (Ln = La, Nd, Sm, and Eu) pyrochlore. *Inorg. Chem. Commun.* **2021**, *127*, 1–10. [[CrossRef](#)]
33. Huang, Z.; Li, F.; Jiao, C.; Liu, J.; Huang, J.; Lu, L.; Zhang, H.; Zhang, S. Molten salt synthesis of La<sub>2</sub>Zr<sub>2</sub>O<sub>7</sub> ultrafine powders. *Ceram. Int.* **2016**. [[CrossRef](#)]
34. Karabaş, M.; Bal, E. New generation thermal barrier coating materials. *Electron. J. Mach. Technol.* **2015**, *12*, 57–64.
35. Itoh, Y.; Saitoh, M. Mechanical properties of overaluminized MCrAlY coatings at room temperature. *J. Eng. Gas Turbines Power* **2005**, *127*, 807–813. [[CrossRef](#)]